High-precision state of charge estimation of urban-road-condition lithium-ion batteries based on optimized high-order term compensation-adaptive extended Kalman filtering.

FENG, R., WANG, S., YU, C., ZHOU, H. and FERNANDEZ, C.

2023

High-Precision State of Charge Estimation of Urban-Road-Condition Lithium-Ion Batteries Based on Optimized High-Order Term Compensation-Adaptive Extended Kalman Filtering

SCHOLARONE™
Manuscripts

1
2
3
4
5
6
7
8
9
10
11
12
13
14
15
16
17
18
19
20
21
22
23
24
25
26
27
28
29
30
31
32
33
34
35
36
37
38
39
40
41
42
43
44
45
46
47
48
49
50
51
52
53
54
55
56
57
58
59
60

High-Precision State of Charge Estimation of Urban-Road-Condition Lithium-Ion Batteries Based on Optimized High-Order Term Compensation-Adaptive Extended Kalman Filtering

Renjun Feng,[1] Shunli Wang,[1,2,z] Chunmei Yu,[1] Heng Zhou,[1] and Carlos Fernandez[3]

[1]School of Information Engineering, Southwest University of Science and Technology, Mianyang 621010, China

[2]School of Electrical Engineering, Sichuan University, Chengdu 610065, China

[3]School of Pharmacy and Life Sciences, Robert Gordon University, Aberdeen, United Kingdom

[z]E-mail: wangshunli1985@qq.com

Abstract

It is significant to improve the accuracy of estimating the state of charge (SOC) of lithium-ion batteries under different working conditions on urban roads. In this study, an improved second-order polarized equivalent circuit (SO-PEC) modeling method is proposed. Accuracy test using segmented parallel exponential fitting parameter identification method. Online parameter identification using recursive least squares with variable forgetting factors(VFFRLS). An optimized higher-order term compensation-adaptive extended Kalman filter (HTC-AEKF) is proposed in the process of estimating SOC. The algorithm incorporates a noise-adaptive algorithm that introduces noise covariance into the recursive process in real-time to reduce the impact of process noise and observation noise on the accuracy of SOC estimation. Multiple iterations are performed for some of the processes in the extended Kalman filter(EKF) to compensate for the accuracy impact of missing higher-order terms in the linearization process. Model validation results show over 98% accuracy. The results after comparing with the EKF algorithm show a 4.1% improvement in SOC estimation accuracy under Hybrid Pulse Power Characterization(HPPC) working conditions. 2.7% improvement in accuracy in Dynamic Stress Test(DST) working conditions. 2.1% improvement in Beijing Bus Dynamic Stress Test(BBDST) working conditions. The superiority of the algorithm is demonstrated.

1. Introduction

Out of concern for the energy crisis and environmental protection, the development and promotion of new energy vehicles, especially electric vehicles, has made a certain degree of progress and breakthrough [1, 2]. The power lithium-ion battery has the advantages of high single-cell voltage, high energy, long cycle life, low self-discharge rate, and no pollution, which is the core power source of choice for various electric vehicles [3]. The charge state of lithium-ion batteries directly reflects the remaining capacity of the battery, and therefore to a certain extent reflects the range of electric vehicles [4, 5]. Nowadays, with the development of urban transportation systems, various road conditions have emerged to put the performance of lithium-ion batteries to a new test. Accurate estimation of the SOC of lithium-ion batteries under different operating conditions is essential to achieve effective management of battery power, avoid overcharging and discharging of batteries, and extend battery life [6].

Current methods for estimating lithium-ion battery SOC include the ampere-time integration method, open-circuit voltage method, data-driven method, and model-based method [7-9]. The ampere-time integration method is simpler, but the method requires the initial state of the SOC to be accurate, and once the error exists it will keep accumulating, resulting in a lack of accuracy in the estimation results [10-12]. The open-circuit voltage method is a common method used in lithium-ion battery testing experiments, this method is mainly based on the fitted OCV-SOC relationship curve to determine the relevant state of the power lithium-ion battery [13], and it is necessary to ensure that the power battery is in an open-circuit state and resting for too long before estimating the SOC [14, 15]. The data-driven method requires a large amount of experimental data with data training, which is too computationally intensive and difficult to meet the real-time nature of powered vehicles [16-18]. The model-based method includes an electrochemical model and an equivalent circuit model [19, 20]. The electrochemical model is modeled based on the charged ion transfer relationship, but the complex electrochemical partial differential equations are difficult to analyze and calculate [21]. The equivalent circuit model uses a linear transformation parameter method to simulate the nonlinear operating characteristics of the power battery, which has linear characteristics and is easy to implement for calculation [22-24]. From the above study, it is clear that the equivalent circuit-based model is more suitable for real-time online systems. The accuracy of the SOC estimation method based on the extended Kalman filter algorithm is limited by the

accuracy of the battery equivalent model parameters [25]. A variable forgetting factor recursive least squares method is used to update each parameter of the second-order model equivalent circuit in real time [26, 27]. The noise covariance magnitude of the extended Kalman filtering algorithm is constant and cannot be updated in real time according to the changes in the SOC estimation process. The Taylor expansion of the linearization process for nonlinear systems is to discard the higher order terms, resulting in a lack of accuracy [28]. Both of these factors can lead to inaccurate SOC estimation results [29].

In order to solve the above two problems and improve the accuracy of SOC estimation under the condition of multi-road cities. The SO-PEC circuit model was constructed. VFFRLS algorithm is used for model parameter identification. On the basis of the traditional extended Kalman filter, the adaptive process of noise and the iterative calculation of higher-order compensation are added to make up for the original shortcomings of the algorithm.

2. Mathematical Analysis

2.1 The SO-PEC Modelling Method

Battery charging and discharging is a complex nonlinear process. To accurately estimate the remaining battery charge, it is especially important to establish a suitable battery performance model [30]. The Rint model does not take the polarization characteristics into account, so the model accuracy is not sufficient. The PNGV model is only suitable for the analysis of battery characteristics in transient environments [31, 32]. The Thevenin model takes into account the cell polarization effect. The dynamic characteristics are better represented, but the accuracy needs to be improved [33]. Therefore, an RC parallel circuit was added to the Thevenin equivalent circuit model to construct the SO-PEC model. The model consists of two parallel RC circuits, which can simulate the internal polarization reaction of a lithium-ion battery during charging and discharging more realistically. Also, the dynamic and static characteristics of the Li-ion battery can be characterized in this model. The SO-PEC model is shown in Fig 1.
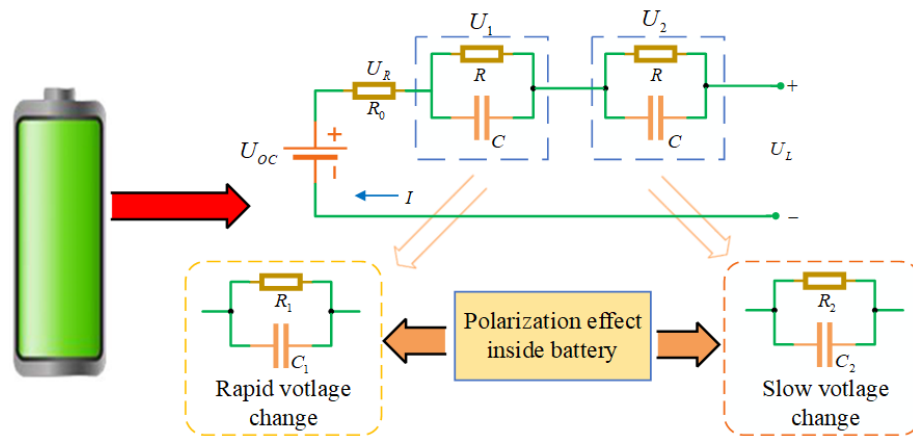
Fig.1 The SO-PEC model

Fig. 1 shows the SO-PEC model, which U_{OC} represents the battery open-circuit voltage, U_L represents the terminal voltage. R_0 is the ohmic internal resistance of the Li-ion battery. U_R indicates the transient voltage drop caused by a sudden change in the current of the lithium-ion battery. The circuit is composed of R_1 and C_1 represents the stage in which the voltage changes rapidly during the chemical reaction inside the battery. The circuit is composed of R_2 and C_2 represents the phase in which the voltage changes slowly during the chemical reaction inside the battery. The terminal voltage U_L in the circuit is shown in Equation (1).

$$U_L = U_{OC} - IR_0 - U_1 - U_2 \tag{1}$$

According to the equivalent model of the second-order circuit shown in Fig.1. According to Kirchhoff's circuit law, the obtained circuit dynamic model is shown in Equation (2).

$$\begin{cases} \left[\dfrac{dU_1}{dt} = -\dfrac{U_1}{R_1 C_1} + \dfrac{I_L}{C_1}\right] \Leftarrow \left\langle I_L = C_1 \dfrac{dU_1}{dt} + \dfrac{U_1}{R_1}\right\rangle \\[2mm] \left[\dfrac{dU_2}{dt} = -\dfrac{U_2}{R_2 C_2} + \dfrac{I_L}{C_2}\right] \Leftarrow \left\langle I_L = C_2 \dfrac{dU_2}{dt} + \dfrac{U_2}{R_2}\right\rangle \end{cases} \tag{2}$$

SOC is defined as the ratio of the remaining capacity of the battery to the rated capacity, and the classical SOC estimation generally uses the ampere-time integration method [34]. The ampere-time integration method estimates the remaining capacity of the battery on the basis of the SOC value at the initial moment [35]. By calculating the integral of the corresponding time of the charge and discharge current within a certain period of time, the percentage change in power can be calculated [36]. The formula of the commonly used ampere-time integration method is shown in Equation (3).

$$SOC = SOC_0 - \frac{1}{Q_n}\int \eta I(t)\Delta t\, dt \tag{3}$$

In Equation (3), SOC_0 is the SOC value of the initial state of the battery. Q_n is the rated capacity of the battery. $I(t)$ represents the magnitude of the discharge current in the circuit. η

represents the Coulomb efficiency, often taken as $\eta \approx 1$ Δt is the sampling period. The SOC is calculated by the ampere-hour integration method, and compared with the SOC value obtained by the HTC-AEKF algorithm.

The parameters SOC, U_1 and U_2 form the parameter matrix $\begin{bmatrix} SOC & U_1 & U_2 \end{bmatrix}^T$ as the state variable[37]. The state space equation and observation equation of lithium-ion battery can be obtained through the above expression, and the calculation process is shown in Equation (4).

$$
\begin{cases}
\begin{bmatrix} SOC(k) \\ U_1(k) \\ U_2(k) \end{bmatrix} = \begin{pmatrix} 1 & 0 & 0 \\ 0 & e^{-\frac{\Delta t}{R_1 C_1}} & 0 \\ 0 & 0 & e^{-\frac{\Delta t}{R_2 C_2}} \end{pmatrix} \begin{bmatrix} SOC(k-1) \\ U_1(k-1) \\ U_2(k-1) \end{bmatrix} + \begin{bmatrix} -\dfrac{\eta \Delta t}{Q_n} \\ R_1\left(1-e^{-\frac{\Delta t}{R_1 C_1}}\right) \\ R_2\left(1-e^{-\frac{\Delta t}{R_2 C_2}}\right) \end{bmatrix} I(k-1) \\
U_L(k) = U_{OC}(k) - U_1(k) - U_2(k) - I(k)R_0
\end{cases}
\tag{4}
$$

2.2 Segment parallel exponential fitting parameter identification

The subject of this experiment is a ternary lithium-ion battery with a rated capacity of 45Ah. But its actual capacity is 43.58Ah. The experiments were conducted using hybrid pulse power characterization (HPPC). This experiment conducts regular charging and discharging of analog circuits within a certain time interval. At this point, it is necessary to record the SOC value of the lithium-ion battery in real time. It is also necessary to record the changes in open circuit voltage and circuit current at each stage. The equation of the state of the equivalent analog circuit is then used to obtain the internal parameters of the circuit. HPPC experimental process is: first of all, the lithium battery is discharged for 10s, left for the 40s, and then charged for 10s, and then left for 40s. The whole process is 1C intermittent constant current discharge of the lithium battery. The voltage and current during charging and discharging of the whole HPPC experiment are shown in Fig.2. Fig.2 shows the HPPC experiments at points where the SOC was between 1.0 and 0.1.

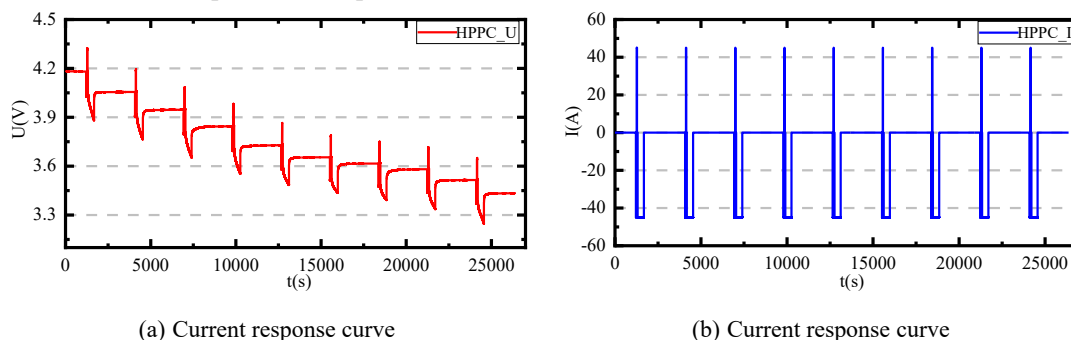(a) Current response curve   (b) Current response curve

Fig. 2 The voltage and current curve of the whole HPPC process.

Fig.3 shows the variation process of charge and discharge voltage at SOC=0.9. In this experiment, there is a violent chemical reaction inside the lithium-ion battery due to the charge and discharge. So the lithium-ion battery needs to be left to stand for 30 minutes after the experiment. It is necessary to wait until the internal chemical and thermal reactions have gradually smoothed out. At this point, SOC = 0.9 read out the voltage value can only be used as the open circuit voltage value. Fig.3 reflects both the transient and steady-state characteristics of the lithium battery. The battery voltage drops instantly at the beginning of the pulse discharge. Then the voltage slowly declines over time during the discharge. When the discharge ends instantly, the battery voltage springs back up immediately. There is a tendency for the voltage to gradually rise back up and level off during the shelving period. The charging process is the opposite of the voltage response of the discharging process.

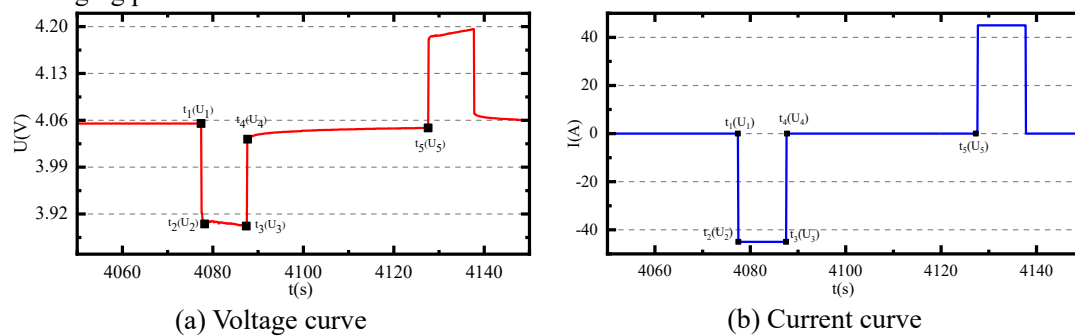(a) Voltage curve   (b) Current curve

Fig. 3 HPPC curve at SOC=0.9

To verify the feasibility and accuracy of the SO-PEC model. At the same time, in order to obtain the variation of external parameters characterizing the operating characteristics of lithium-ion batteries. In this paper, a segmented parallel exponential fitting parameter identification method is proposed. The zero-state response of the charge/discharge phase was selected by segmented parallel exponential fitting at the point of the 10 SOC sections. The simulated voltage calculated from the parameter identification results is compared with the actual voltage of the model, the voltage error of the cross section is analyzed, and the actual characteristics of the model are evaluated. The calculation process of this method is shown below.

In the two time periods of $t_1 \square t_2$ and $t_3 \square t_4$, the ohmic resistance is affected by the sudden change of current, which causes a transient change of voltage. The formula for calculating ohmic resistance is shown in Equation (5).

$$R_0 = \frac{(U_1 - U_2) + (U_4 - U_3)}{2I} \tag{5}$$

During the period t_2 to t_3, the terminal voltage of the battery does not change substantially during this period due to the zero state response. Time domain analysis is performed for the time period from U_2 to U_3. The time-varying functional relationship between U_L and time t is obtained.

$$U_L(t) = U_{OC} - IR_1(1 - e^{-1/\tau_1}) - IR_2(1 - e^{-1/\tau_2}) \tag{6}$$

Equation (5) can be written as a multi-parameter unknown functional relationship, as shown in Equation (7).

$$\begin{cases} y = a^{-\frac{x}{c}} + b^{-\frac{x}{d}} + e \\ R_1 = \dfrac{a}{I}, R_2 = \dfrac{b}{I} \\ C_1 = \dfrac{c}{R_1}, C_2 = \dfrac{d}{R_2} \end{cases} \tag{7}$$

By collecting 10 pulse data under HPPC operating conditions, the parameters a, b, c, d, and e can be fitted in the simulation software. The parameters of the SO-PEC model can be identified through Equation (7).

2.3 Variable Forgetting Factor Recursive Least Squares Method

After the accuracy verification of the SO-PEC model, the VFFRLS algorithm is used for online parameter identification of the model. The VFFRLS algorithm uses a variable forgetting factor adaptive to find the optimal value of the forgetting factor and improve the adaptability of the algorithm [38]. The algorithm's parameter discrimination estimation capability does not overly depend on the current data as the model parameters change in real time [39, 40].

The least squares method is a simple and effective fitting algorithm that can give more accurate parameter fitting results for nonlinear systems, calculated as in Equation (8).

$$y(k) = \ell^T(k)\theta + e(k) \tag{8}$$

In Equation (8), the $y(k)$ is the value of the system output quantity at moment k and $\ell^T(k)$ is the observed quantity. θ is the matrix of the waiting discrimination parameters, $e(k)$ is the estimation error of the RLS Model output comparison verification at moment k. $\ell^T(k)$ and θ are calculated as shown in Equation (9).

$$\begin{cases} \ell^T(k) = [-y(k-1) \cdots -y(k-n)u(k) \cdots u(k-n)] \\ \theta = [a_1 a_2 \cdots a_n b_1 b_2 \cdots b_n] \end{cases} \tag{9}$$

In the above Equation (9), the $u(k)$ is the input value of the system at k times. The criterion function $J(\theta)$ is shown in Equation (10).

$$J(\theta) = \sum_{k=1}^{\infty} [e(k)]^2 = [y(k) - \ell^T(k)\theta]^T [y(k) - \ell^T(k)\theta] \tag{10}$$

When $J(\theta)$ taking the minimum value, the least squares estimate is obtained. The estimation is calculated as shown in Equation (11).

$$\hat{\theta} = \left[\ell^T(k)\ell(k) \right]^{-1} \ell(k)y(k) \tag{11}$$

The above Equation (8) ~ (11) is the derivation process of parameter identification of the RLS algorithm. RLS has a short memory time. As the number of recursions increases, historical data continues to accumulate, and it is difficult to correct the new data that follows. Therefore, it is necessary to add a forgetting factor to weaken data saturation.

The recursive correction of the forgetting factor is introduced, and the specific formula is shown in Equation (12).

$$\begin{cases} \hat{\theta}(k+1) = \hat{\theta}(k) + K(k+1)\left[y(k+1) - \ell^T(k+1)\hat{\theta}(k) \right] \\ K(k+1) = P(k)\ell(k+1)\left[\lambda + \ell^T(k+1)P(k)\ell(k+1) \right]^{-1} \\ \quad P(k+1) = \frac{1}{\lambda}\left[I - K(k+1)\ell^T(k+1) \right]P(k) \end{cases} \tag{12}$$

From this, the RLS algorithm was improved into the FFRLS algorithm. In Equation (12), $K(k+1)$ is the gain of the operation at k-time and $P(k+1)$ is the covariance at $k+1$. λ is the forgetting factor, in general, λ =0.98, but this is only an empirical value. It cannot adjust the size of the value in time according to the recognition error. This is the main cause of FFRLS parameter identification errors. It is necessary to improve the time variability of the forgetting factor[41, 42].

The following recursive formula for adding the variable forgetting factor to the FFRLS is shown in (13) and (14).

$$L(k) = -\rho \frac{\sum_{i=k-M+1}^{k} e_i e_i^2}{M} \tag{13}$$

Equation (13), e_i the estimation error at moment i and M is the window size . ρ is the Sensitive factor. The calculation formula of the variable forgetting factor is shown in Equation (14).

$$\lambda(k) = \lambda_{min} + (\lambda_0 - \lambda_{min}) \cdot 2^{L(k)} \tag{14}$$

A large or small value of the forgetting factor can cause a decrease in the estimation accuracy of the algorithm. If the adaptive value of the forgetting factor is taken close to the value 1, the algorithm cannot keep track of the changes in the model parameters in time. If the forgetting factor approaches the value 0, the data of the current moment will dominate. This can weaken the ability of the algorithm to discriminate the model parameters. The algorithm will have a lag effect. λ_{min} is the minimum value of the forgetting factor. $\lambda(k)$ is the value of the forgetting factor at the moment k. To prevent $\lambda(k)$ from taking a value of 1, replace 1 in the formula with a constant λ_0 less than

1. The value $\lambda(k)$ is determined by the mean squared value of the estimation error of M sample points before the present moment k.

2.4 High-order Term Compensation-Adaptive Extended Kalman Filtering

The extended Kalman filter has two disadvantages. On the one hand, the extended Kalman filtering algorithm is cyclically iterative. The process noise covariance Q_k and the measurement noise covariance R_k are usually treated as constant values. However, nonlinear systems usually operate with disturbances. The values of these two covariances are always changing. Therefore, it causes inaccurate estimation of SOC of Li-ion battery and the estimation accuracy is not up to the requirement. On the other hand, the extended Kalman filter discards higher order terms during the Taylor series expansion of the linearization of the nonlinear system, but at the same time causes a lack of estimation accuracy [43].

To solve these two problems it is necessary to improve the traditional Kalman filtering algorithm. To resolve the error caused by constant noise covariance. In this paper, the adaptive noise algorithm is introduced on the basis of the original Kalman filter. The noise covariance is added as a variable to the iterative process that is continuously updated. Regarding the loss of estimation accuracy caused by discarding higher-order terms in the linearization process. In this paper, iterative computation is used to repeat some of the processes of the extended Kalman filtering algorithm. At the end of each cycle, the values of the posterior estimates are reintroduced into the observation equation to obtain the new Jacobi matrix. This method reuses the collected information to make the estimated value closer to the true value.

Kalman filter is usually used for linear systems or nonlinear systems, the Kalman filter needs to be discretized, and the discretized spatial equation of state is shown in Equation (15).

$$\begin{cases} x_k = A_k x_{k-1} + B_k u_{k-1} + w_k \\ y_k = C_k x_k + D_k u_k + v_k \end{cases} \tag{15}$$

The equations above are the system state equation and the measurement equation, which x_k represents the system state at moment k. x_{k-1} is the system state at moment $k-1$. u_{k-1} is the system input at moment $k-1$. y_k is the system process noise. v_k is the observation noise. A_k represents the transfer matrix to describe the mapping between the system states between the before and after moments. B_k represents the input matrix to represent the effect of external inputs on the system. C_k is the output matrix to describe the effect of state vectors on the observations. D_k is the feedforward matrix to describe the effect of external inputs on the predicted observations.

The system state space equations of the extended Kalman filter algorithm can be expressed as Equation (16).

$$\begin{cases} x_k = f\left(x_{k-1}, u_k\right) + w_k \\ y_k = h\left(x_k, u_k\right) + v_k \end{cases} \tag{16}$$

In Equation (16), $f\left(x_{k-1}, u_k\right)$ the system equation of state $h\left(x_k, u_k\right)$ is the system equation of observation. w_k and v_k are independent Gaussian white noises and are not correlated with each other, Q_k and R_k are the covariances of w_k and v_k, respectively.

The following is the specific calculation procedure of the high-order term compensation-adaptive extended Kalman filtering algorithm.

(1) The initialization formula is shown in Equations (17). P_0^+ is the mean square deviation matrix, $\hat{x}_0^+$ is the state variable.

$$\begin{cases} \hat{x}_0^+ = E\left[x_0\right] \\ P_0^+ = E\left[\left(x_0 - \hat{x}_0^+\right)\left(x_0 - \hat{x}_0^+\right)^T\right] \end{cases} \tag{17}$$

(2) The Jacobian matrix formula for calculating the equation of state is shown in Equation (18).

$$A_{k-1} = \frac{\partial f\left(x_{k-1}^-, u_k\right)}{\partial x} \tag{18}$$

(3) The error update formula of state variable and mean square estimation is shown in Equation (19).

$$\begin{cases} \hat{x}_k^- = f\left(\hat{x}_{k-1}, u_{k-1}\right) \\ P_k^- = A_{k-1} P_{k-1}^+ A_{k-1}^T + Q_k \end{cases} \tag{19}$$

In Equation (19), $\hat{x}_k^-$ represents the prior estimate of the state variable at moment k. P_k^- represents the prior error estimation of the covariance matrix at moment k.

(4) for i= 1:c, the calculation of the i-th iteration is shown in Equation (20).

$$\begin{cases} \hat{x}_k^{-i} = f\left(\hat{x}_{k-1}^{+i}, u_{k-1}\right) \\ p_k^{-i} = A_{k-1}^i P_{k-1}^+ A_{k-1}^{Ti} + Q_k \end{cases} \tag{20}$$

In Equation (20), $\hat{x}_k^{-i}$ is the i-th a priori estimate of the state variable $\hat{x}_k^-$ at this moment in time k. $\hat{x}_{k-1}^{+i}$ is the posterior estimate of the state variable $\hat{x}_{k-1}^-$ at moment $k-1$. u_{k-1} is the input current at moment $k-1$. p_k^{-i} is the i-th a priori estimate of the covariance at moment k.

The estimation error of the state variable is not guaranteed to decrease continuously in the iterative calculation process due to the presence of uncertainties such as noise, so the prediction covariance matrix needs to be adjusted. Therefore, the covariance during each round of iterations can be rectified by finding a damping factor ω of the suitable size to reduce the error and improve the accuracy, and the specific adjustment formula is shown in Equation (21).

$$\hat{P}_k^{-i} = \left[I - p_k^{-i}\left(p_k^{-i} + \frac{1}{\omega} I_b\right)\right] p_k^{-i} \tag{21}$$

(5) Calculate the Jacobi matrix of the observation equation as shown in Equation (22).

$$C_k^i = \frac{\partial h(\hat{x}_k^+)}{\partial x} \tag{22}$$

(6) The gain matrix is shown in Equation (23), where L_k^i is the Kalman gain.

$$L_k^i = \frac{P_k^{-i} C_k^{iT}}{C_k^i P_k^{-i} C_k^{iT} + R_k} \tag{23}$$

(7) The optimal estimation of state variables is shown in Equation (24).

$$\hat{x}_k^{+i} = \hat{x}_k^{-i} + L_k^i \left[y_k - h(\hat{x}_k^{-i}, u_k) \right] \tag{24}$$

(8) The mean square deviation optimal estimate is shown in Equation (25).

$$P_k^{+i} = \left(I - L_k^i C_k^i \right) \hat{P}_k^{-i} \tag{25}$$

(9) Get the calculation result.

When the number of iterations in a single step period reaches the set threshold c or the difference between the estimated values of successive iterations is less than the preset threshold ϖ, the iteration process is exited. Continue the recursive calculation at the time of $k-1$, and input the final state variable $\hat{x}_k^+$ and covariance estimate P_k^+ at the time of k, as shown in Equation (26).

$$\begin{cases} \hat{x}_k^+ = \hat{x}_k^{+i} \\ P_k^+ = P_k^{+i} \end{cases} \tag{26}$$

(10) The noise adaptive algorithm is shown in Equation (27).

$$\begin{cases} Q_{k+1}^i = L_k A_{k-1}^i L_k^T \\ e_i = y_k - h(\hat{x}_k^{-i}, u_k) \\ F_k^i = \frac{1}{M} \sum_{j=i-M-1}^{i} e_i e_i^T \\ R_{k+1}^i = F_k^i + C_k^i P_k^{-i} C_k^{iT} \end{cases} \tag{27}$$

In Equation (27), Q_{k+1}^i is the iterative value of the process noise covariance for update Equation (20). R_{k+1}^i is an iterative value that measures the noise covariance for the updated Equation (23). e_i is the difference between the true value and the predicted value of the algorithm. M is the matching window size. The algorithm flow is shown in Fig.4.

In this paper, root means square error (RMSE) and mean absolute error (MAE) are used as metrics for judging the accuracy of the algorithm. Evaluate whether the algorithm meets the accuracy improvement requirements. $SOC'(t)$ is the estimated value, and $SOC(t)$ is the calculated value of the ampere-hour integral. N is the total number of data.

$$RMSE = \sqrt{\frac{\sum_{t=1}^{N} (SOC'(t) - SOC(t))^2}{N}} \tag{28}$$

$$MAE = \frac{\sum_{t=1}^{N}\left|\left(SOC'(t) - SOC(t)\right)\right|}{N} \qquad (29)$$

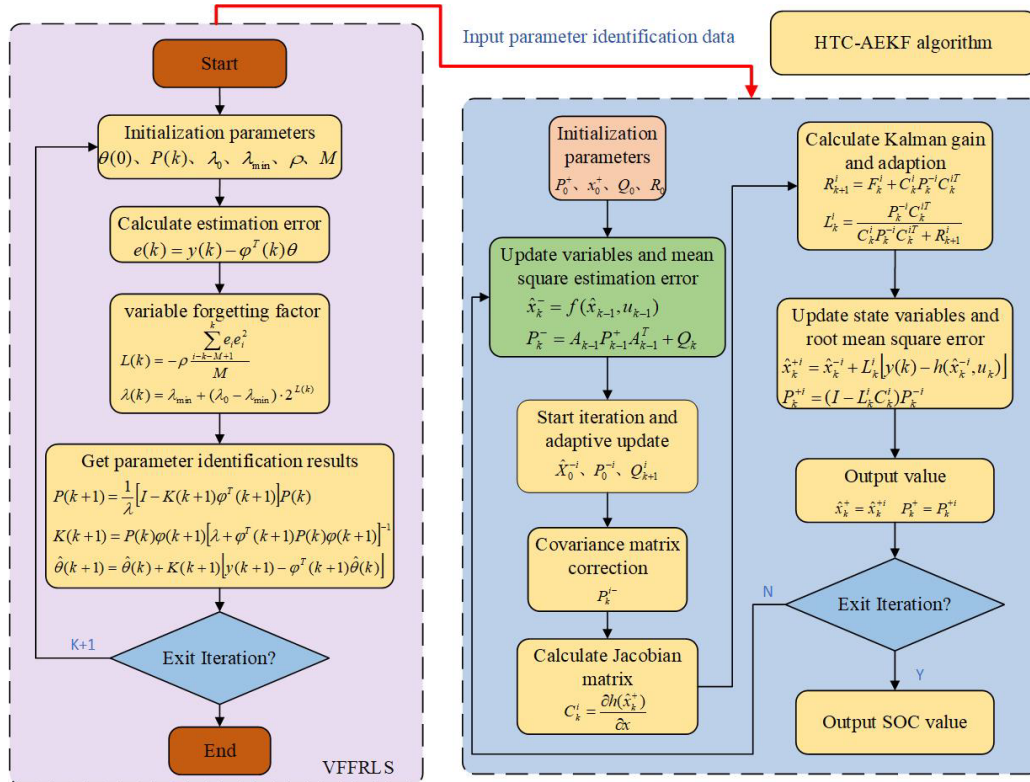Fig. 4 Algorithm flow chart of parameter identification and SOC estimation

3. Analysis of results

3.1 Experimental platform construction

During the data analysis and processing, valid data segments are extracted from the original experimental data. Then, the data segments are sampled in an effective manner. Finally, the relationship between the internal parameters of the SO-PEC model and the SOC data collected from the experiment was obtained. So as to achieve an accurate description of the working characteristics of the lithium battery. The experimental process is shown in Fig.5.
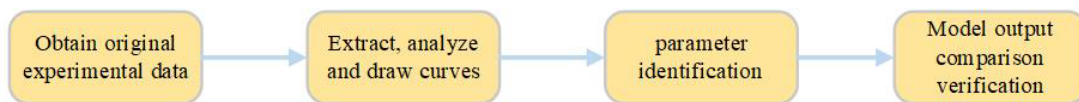
Fig. 5 Data processing and model validation

The experimental data for HPPC, DST, and BBDST working conditions were measured on the following experimental platform. The experimental platform is shown in Fig.6.
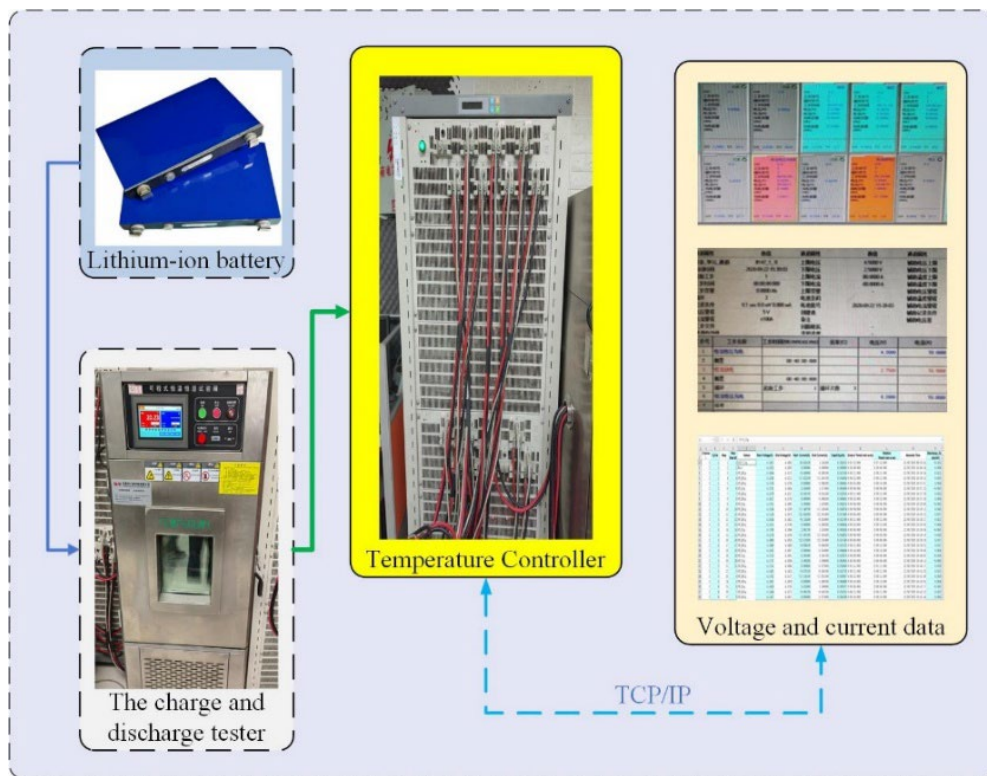
Fig. 6 Experimental test platform

In order to obtain more accurate experimental data, the BTS200-100-104 instrument was used in this experiment. This device includes battery data testing equipment and temperature control devices. The function of a computer terminal is to control the working conditions setting, charging and discharging, and testing data collection of testing equipment. The function of a thermostat is to maintain a constant temperature in the testing environment during lithium-ion battery testing. The original data of DST and BBDST are shown in Fig. 7 and Fig.8.
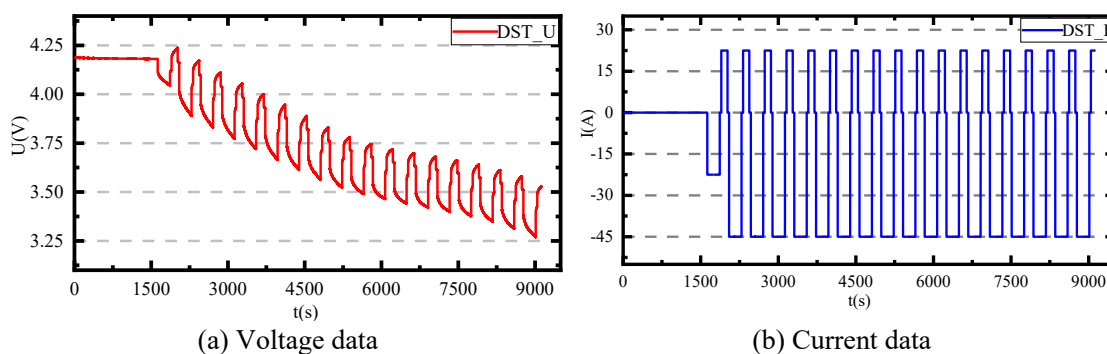

(a) Voltage data

(b) Current data

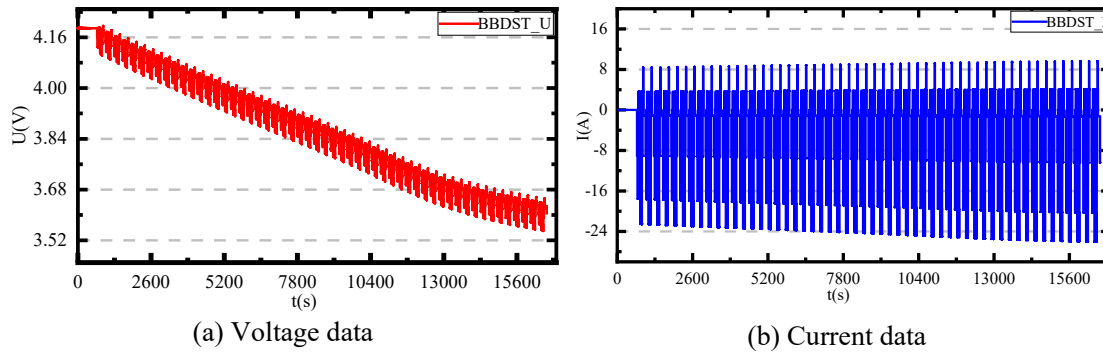Fig. 7 DST measurement data

(a) Voltage data

(b) Current data

Fig. 8 BBDST measurement data

3.2 SO-PEC model accuracy validation

A 30-minute window period should be set after the end of each cycle in this experiment. The purpose of doing so is to ensure that the electrochemical and thermal reactions inside the lithium-ion battery become stable. The experimental conclusion drawn in this way is more convincing. The SOC values for this HPPC operating condition were taken from 10 points. The identification results of each parameter of the SO-PEC model are shown in Table 1.

Table.1 Results of the model parameters.

$SOC(100\%)$	$U_{OC}(V)$	$R_0(\Omega)$	$R_1(\Omega)$	$R_2(\Omega)$	$C_1(F)$	$C_2(F)$
1	4.184	0.002412	0.001688	0.0001	5997	1.026e+06
0.9	4.057	0.002160	0.001203	0.0001167	8707	8.71e+05
0.8	3.949	0.002552	0.001871	0.0001	5003	9.257e+05
0.7	3.847	0.002105	0.001191	0.0001	8048	1.206e+06
0.6	3.723	0.002749	0.001239	0.000259	7092	3.915e+05
0.5	3.657	0.002372	0.001141	0.0001003	6749	9.251e+05
0.4	3.618	0.002669	0.001086	0.0001001	9092	1.056e+06
0.3	3.585	0.002011	0.001291	0.001064	8841	9.63e+04
0.2	3.544	0.002849	0.001009	0.000163	10090	1.127e+06
0.1	3.378	0.001258	0.001141	0.0001	6093	4.171e+06

The data shown in Table 1 is imported into the simulation software and the equivalent circuit model is simulated. Obtain the simulated voltage for the SO-PEC model. The simulated voltage of the model is then compared with the actual voltage. To identify whether the model has high accuracy. The voltage and actual voltage comparison graph and error graph are shown in Fig.9.

(a) Terminal voltage comparison diagram

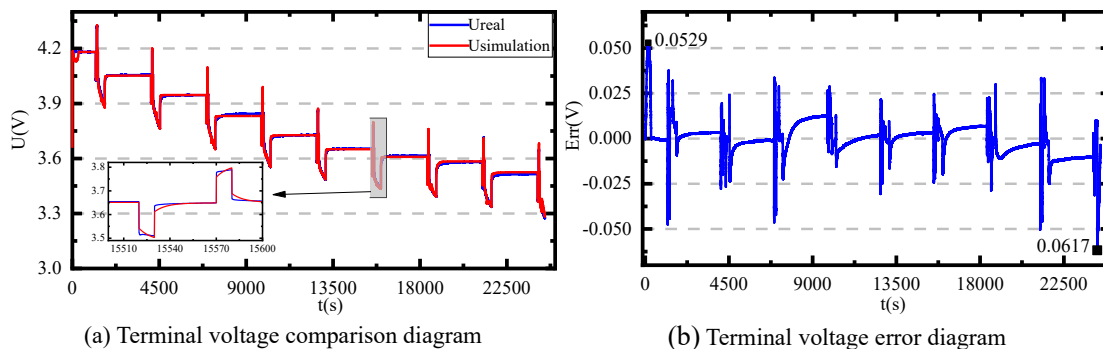(b) Terminal voltage error diagram

Fig. 9 Parameter identification results under HPPC working conditions

From Fig.9, it can be seen that the maximum error between the actual voltage and the simulated voltage is 0.0617V. The accuracy of the model reaches 98.25%. The calculation formula is shown in Equation (30).

$$E_{rr} = \frac{U_{rr}}{U_{OC,1}} \tag{30}$$

E_{rr} is the estimation accuracy. U_{rr} is the value of the estimation error. $U_{OC,1}$ is the open-circuit voltage when the SOC is 1.

3.3 Validation of VFFRLS parameter identification results

After verification of model feasibility and accuracy, in order to verify the accuracy of the VFFRLS online parameter identification results, the experimental data of DST and BBDST working conditions were extracted at the end of the working condition experiment. Through the iterative calculation of online parameter identification, the parameter identification results of the SO-PEC equivalent circuit model are obtained. The voltage error is obtained by comparing the actual terminal voltage of each working condition with the analog voltage. The results are shown in Fig.10 and Fig.11.
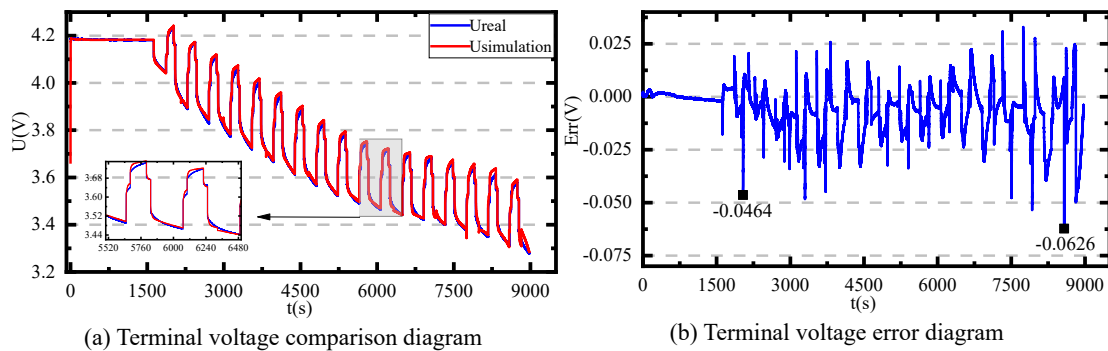

| (a) Terminal voltage comparison diagram | (b) Terminal voltage error diagram |

Fig.10 Parameter identification results under DST working conditions

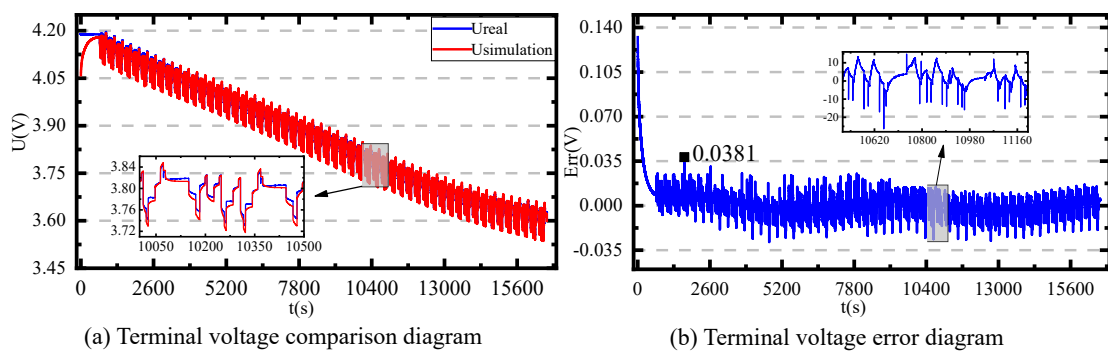| (a) Terminal voltage comparison diagram | (b) Terminal voltage error diagram |

Fig.11 Parameter identification results under BBDST working conditions

The maximum error of the terminal voltage in the DST working condition is 6.26%, and the maximum error of the terminal voltage in the BBDST working condition is 3.81%, which can be

controlled within the allowed error range. The VFFRLS method matches the analog voltage well with the true terminal voltage for each working condition. It is shown that the method can adaptively adjust the value of the forgetting factor according to the magnitude of the estimation error in the parameter identification process to avoid data oversaturation. The purpose of improving the accuracy of parameter identification is achieved. Table 2 shows the error data analysis results of DST and BBDST working conditions.

Table 2. Identification results of DST and BBDST working conditions parameters.

Working conditions	MAXErr	MAE	RMSE
DST	-6.26%	0.95%	0.72%
BBDST	3.18%	1.12%	1.01%

It can be seen from Table 2 that the mean absolute error under DST working conditions is 0.95%. This indicates a high degree of fit between predicted and true values. The root means square error is only 0.72%. Under BBDST working conditions, the mean absolute error is 1.12%. The root means square error is 1.01%.

## 3.4 Validation of SOC estimation results with HTC-AEKF algorithm

After the model validation in section 3.2, the SO-PEC model proposed in this paper can accurately characterize the operating state of the lithium-ion battery. The parameter identification results in section 3.3 show that the online parameter identification accuracy of the VFFRLS algorithm meets the requirements. Next, the accuracy of the SOC estimation of the HTC-AEKF algorithm needs to be verified under HPPC operating conditions, DST operating conditions, and BBDST operating conditions. The initial error of the algorithm is also set to 10% and 50% to verify the robustness of the algorithm. To check whether the HTC-AEKF algorithm can meet the improvement requirements. It is examined whether the adaptive algorithm and the higher-order compensation algorithm can improve the accuracy of SOC estimation. The estimation results and estimation errors are shown in Fig.12, Fig.13, and Fig.14.
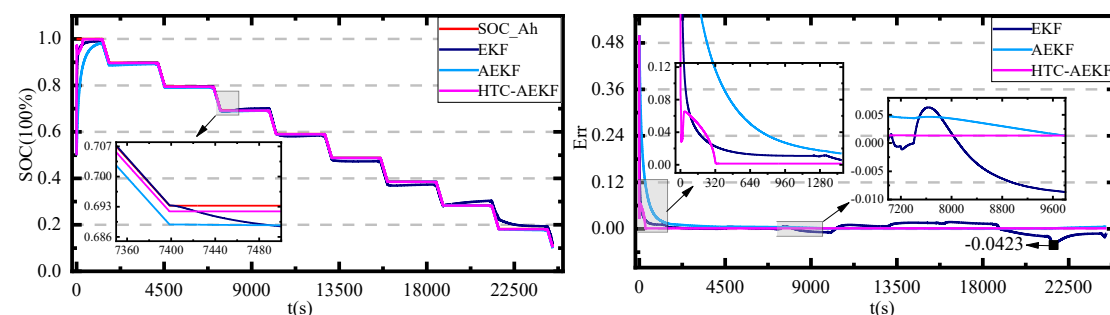
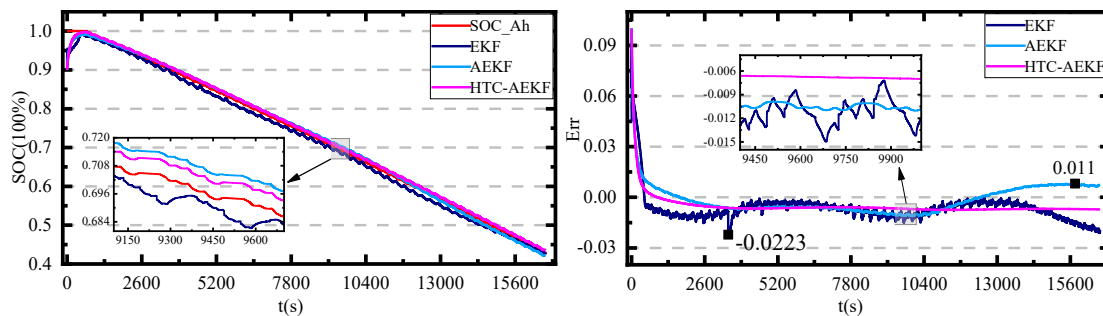(a) Graph of SOC estimation results   (b) Error plot of SOC estimation

Fig.12 SOC estimation results under HPPC working condition
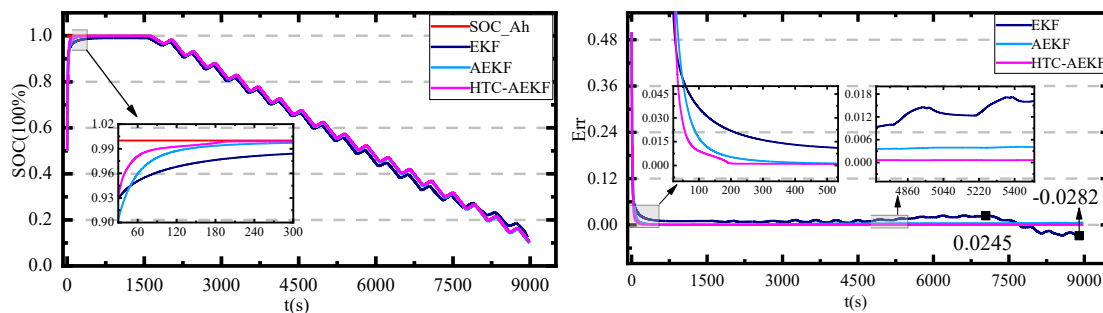
(a) Graph of SOC estimation results

(b) Error plot of SOC estimation

Fig.13 SOC estimation results under DST working condition

(a) Graph of SOC estimation results

(b) Error plot of SOC estimation

Fig.14 SOC estimation results under BBDST working condition

Fig.12 shows the SOC estimation results of the HTC-AEKF algorithm for the HPPC working condition. Fig.13 shows the SOC estimation results of the HTC-AEKF algorithm for the DST working condition. Fig.14 shows the SOC estimation results of the HTC-AEKF algorithm for the BBDST working condition. The convergence speed of the HTC-AEKF algorithm is significantly faster and the convergence time is shorter than that of the EKF and AEKF algorithms, as can be seen from the three working condition result plots. At initial errors of 10% and 50%, the algorithm still converges quickly to the vicinity of the value of the Ansatz integral, demonstrating its robustness.

From Fig.14, it can be learned that the EKF algorithm shows a large algorithm error at the beginning of the discharge, with the error reaching 2.23% at one point. The main reason for the large error is the failure to find a suitable noise covariance when noise is involved in the recursion at the beginning of the algorithm. This situation affects the accuracy of the Kalman gain and leads to an increase in the algorithm error. The error continuously starts to converge under the correction of the observations and the error remains stable in the later stages of the algorithm. In contrast, the AEKF algorithm shows large fluctuations in the late stage of SOC estimation, which is caused by the fact that the AEKF algorithm does not compensate for the missing higher-order terms in the linearization of the nonlinear system. The comparison of data obtained from the improved algorithm in Table 3 can also further illustrate the advantages of the algorithm.

Table 3. Estimation results of EKF, AEKF, and HTC-AEKF algorithms.

Working conditions	Algorithm	MAXErr	MAE	RMSE
HPPC	EKF	-4.23%	1.05%	1.65%
	AEKF	0.62%	0.42%	0.52%
	HTC-AEKF	0.13%	0.11%	0.12%
DST	EKF	2.82%	1.46%	2.12%
	AEKF	0.58%	0.41%	0.48%
	HTC-AEKF	0.12%	0.10%	0.11%
BBDST	EKF	2.23%	0.87%	1.12%
	AEKF	1.10%	0.72%	0.92%
	HTC-AEKF	0.74%	0.64%	0.66%

As shown in Table 3, compared with the EKF algorithm and AEKF algorithm, the maximum error of SOC estimation of the HTC-AEKF algorithm decreased by 4.1% and 0.49% respectively under HPPC conditions. The average absolute error of the algorithm is only 0.11%, and the root mean square error is only 0.12%. This shows that the algorithm still has strong robustness and estimation accuracy when the initial error is 50%. Under the DST condition, the maximum SOC estimation error of the HTC-AEKF algorithm is less than 0.12%, which is far less than the SOC estimation error of the EKF and AEKF algorithms. Compared with EKF and AEKF algorithms, the average absolute error decreases by 1.36% and 0.31% respectively. This shows that the SOC prediction value of the algorithm is closer to the real value, and the prediction accuracy of the algorithm is higher. The root means square error is only 0.11%. Under the BBDST condition, the maximum error of the HTC-AEKF algorithm is not more than 0.74%, which is 0.36% less than that of the AEKF algorithm. The average absolute error is only 0.64%, and the root mean square error is reduced by 0.46% and 0.26% respectively compared with EKF and AEKF. The above results show that HTC-AEKF has strong accuracy and the algorithm has been improved.

4. Conclusion

This paper presents a method that enables accurate estimation of the SOC of lithium-ion batteries. The following is the main work made in this paper and the innovation points.

(1). In order to obtain the variation of external parameters characterizing the operating properties of lithium-ion batteries, a SO-PEC model is proposed in this paper. The accuracy of the model was verified using the parameter identification method of segmented parallel exponential fitting.

(2). After the model feasibility and accuracy verification, the VFFRLS algorithm is used to identify the parameters of the model. The identification results show that the average absolute error is only 0.95% in the DST working condition. The maximum error between real and simulated voltage does not exceed 3.18% under BBDST working conditions. The average absolute error does not exceed 1.12%.

(3). For errors caused by the loss of higher order terms due to the linearization process. This paper proposes to introduce an iterative computation method to perform some processes in the classical extended Kalman filtering algorithm multiple times. The HTC-AEKF algorithm is obtained by improving it in this way. The results show that the maximum SOC estimation error does not exceed 0.74% for HPPC, DST, and BBDST working conditions.

In summary, the HTC-AEKF algorithm proposed in this study can accurately estimate the SOC of lithium-ion batteries. It has a strong practicality to detect and estimate the battery status of electric vehicles in real-time under different road working conditions. This has important implications for extending battery life and improving driving safety.

Acknowledgments

Reference

1. Adaikkappan, M., & Sathiyamoorthy, N., *A real time state of charge estimation using Harris Hawks optimization-based filtering approach for electric vehicle power batteries*. INTERNATIONAL JOURNAL OF ENERGY RESEARCH, 2022. 46(7): p. 9293-9309.

2. Al-Gabalawy, M., Hosny, N. S., Dawson, J. A., & Omar, A. I., *State of charge estimation of a Li-ion battery based on extended Kalman filtering and sensor bias*. INTERNATIONAL JOURNAL OF ENERGY RESEARCH, 2021. 45(5): p. 6708-6726.

3. Du, B. H., Yu, Z., Yi, S. H., He, Y. L., & Luo, Y. L., *State-of-charge estimation for second-life lithium-ion batteries based on cell difference model and adaptive fading unscented Kalman filter algorithm*. INTERNATIONAL JOURNAL OF LOW-CARBON TECHNOLOGIES, 2021. 16(3): p. 927-939.

4. Fang, Y. Y., Zhang, Q., Zhang, H., Xu, W. C., Wang, L. S., Shen, X. L., Yun, F. L., Cui, Y., Wang, L., & Zhang, X., *State-of-charge estimation technique for lithium-ion batteries by means of second-order extended Kalman filter and equivalent circuit model: Great temperature robustness state-of-charge estimation*. IET POWER ELECTRONICS, 2021. 14(8): p. 1515-1528.

5. Feng, L., Ding, J., & Han, Y. Y., *Improved sliding mode based EKF for the SOC estimation of lithium-ion batteries*. IONICS, 2020. 26(6): p. 2875-2882.

6. Haus, B., & Mercorelli, P., *Polynomial Augmented Extended Kalman Filter to Estimate the State of Charge of Lithium-Ion Batteries*. IEEE TRANSACTIONS ON VEHICULAR TECHNOLOGY, 2020. 69(2): p. 1452-1463.

1
2
3
4
5
6
7
8
9
10
11
12
13
14
15
16
17
18
19
20
21
22
23
24
25
26
27
28
29
30
31
32
33
34
35
36
37
38
39
40
41
42
43
44
45
46
47
48
49
50
51
52
53
54
55
56
57
58
59
60

7. Havangi, R., *Adaptive robust unscented Kalman filter with recursive least square for state of charge estimation of batteries*. ELECTRICAL ENGINEERING, 2022. 104(2): p. 1001-1017.

8. He, L., Hu, M. K., Wei, Y. J., Liu, B. J., & Shi, Q., *State of charge estimation by finite difference extended Kalman filter with HPPC parameters identification*. SCIENCE CHINA-TECHNOLOGICAL SCIENCES, 2020. 63(3): p. 410-421.

9. Hou, J., Yang, Y., & Gao, T., *A Variational Bayes Based State-of-Charge Estimation for Lithium-Ion Batteries Without Sensing Current*. IEEE ACCESS, 2021. 9: p. 84651-84665.

10. Huang, Z. J., Fang, Y. S., & Xu, J. J., *SOC ESTIMATION OF Li-ION BATTERY BASED ON IMPROVED EKF ALGORITHM*. INTERNATIONAL JOURNAL OF AUTOMOTIVE TECHNOLOGY, 2021. 22(2): p. 335-340.

11. Ji, Y. J., Qiu, S. L., & Li, G., *Simulation of second-order RC equivalent circuit model of lithium battery based on variable resistance and capacitance*. JOURNAL OF CENTRAL SOUTH UNIVERSITY, 2020. 27(9): p. 2606-2613.

12. Jiang, C., Wang, S. L., Wu, B., Etse-Dabu, B., & Xiong, X., *A Novel Adaptive Extended Kalman Filtering and Electrochemical-Circuit Combined Modeling Method for the Online Ternary Battery state-of-charge Estimation*. International Journal Of Electrochemical Science, 2020. 15(10): p. 9720-9733.

13. Lei, G. P., Luo, X. Y., Cai, L., Gao, L., Dai, N. N., Xu, Q. S., & Tan, Z. F., *Research on smart EFK algorithm for electric vehicle battery packs management system*. JOURNAL OF INTELLIGENT & FUZZY SYSTEMS, 2020. 38(1): p. 257-262.

14. Li, J. B., Ye, M., Gao, K. P., Jiao, S. J., & Xu, X. X., *State estimation of lithium polymer battery based on Kalman filter*. IONICS, 2021. 27(9): p. 3909-3918.

15. Li, W. Q., Yang, Y., Wang, D. Q., & Yin, S. Q., *The multi-innovation extended Kalman filter algorithm for battery SOC estimation*. IONICS, 2020. 26(12): p. 6145-6156.

16. How, D. N. T., Hannan, M. A., Lipu, M. S. H., Sahari, K. S. M., Ker, P. J., & Muttaqi, K. M., *State-of-Charge Estimation of Li-Ion Battery in Electric Vehicles: A Deep Neural Network Approach*. IEEE TRANSACTIONS ON INDUSTRY APPLICATIONS, 2020. 56(5): p. 5565-5574.

17. Zhao, F., Li, Y. G., Wang, X. H., Bai, L., & Liu, T. L., *Lithium-Ion Batteries State of Charge Prediction of Electric Vehicles Using RNNs-CNNs Neural Networks*. IEEE ACCESS, 2020. 8: p. 98168-98180.

18. Shu, X., Li, G., Zhang, Y. J., Shen, S. Q., Chen, Z., & Liu, Y. G., *Stage of Charge Estimation of Lithium-Ion Battery Packs Based on Improved Cubature Kalman Filter With Long Short-Term Memory Model*. IEEE TRANSACTIONS ON TRANSPORTATION ELECTRIFICATION, 2021. 7(3): p. 1271-1284.

19. Zhang, Z. Y., Jiang, L., Zhang, L. Z., & Huang, C. X., *State-of-charge estimation of lithium-ion battery pack by using an adaptive extended Kalman filter for electric vehicles*. JOURNAL OF ENERGY STORAGE, 2021. 37: p. 654-720.

20. Zhang, S. Z., & Zhang, X. W., *A comparative study of different online model parameters identification methods for lithium-ion battery*. SCIENCE CHINA-TECHNOLOGICAL SCIENCES, 2021. 64(10): p. 2312-2327.

21. Xu, J. Y., & Wang, D. Q., *A dual-rate sampled multiple innovation adaptive extended Kalman filter algorithm for state of charge estimation*. INTERNATIONAL JOURNAL OF ENERGY RESEARCH, 2022. 46(13): p. 18796-18808.

22. Xiong, W., Mo, Y. M., & Zhang, F., *Identification of Parameters in Li-Ion Battery Model by Least Squares Method with Variable Forgetting Factor*. INTERNATIONAL JOURNAL OF COMPUTATIONAL METHODS, 2020. 17(7): p. 10056-10090.

23. Wang, Q. T., & Qi, W., *New SOC estimation method under multi-temperature conditions based on parametric-estimation OCV*. JOURNAL OF POWER ELECTRONICS, 2020. 20(2): p. 614-623.

24. Wang, B., Qin, F. F., Zhao, X. B., Ni, X. P., & Xuan, D. J., *Equalization of series connected lithium-ion batteries based on back propagation neural network and fuzzy logic control*. INTERNATIONAL JOURNAL OF ENERGY RESEARCH, 2020. 44(6): p. 4812-4826.

25. Luo, Y., Qi, P. W., Kan, Y. Z., Huang, J. Y., Huang, H., Luo, J. W., Wang, J. N., Wei, Y. H., Xiao, R. J., & Zhao, S., *State of charge estimation method based on the extended Kalman filter algorithm with consideration of time-varying battery parameters*. INTERNATIONAL JOURNAL OF ENERGY RESEARCH, 2020. 44(13): p. 10538-10550.

26. Ouyang, Q., Ma, R., Wu, Z. X., Xu, G. T., & Wang, Z. S., *Adaptive Square-Root Unscented Kalman Filter-Based State-of-Charge Estimation for Lithium-Ion Batteries with Model Parameter Online Identification*. ENERGIES, 2020. 13(18): p. 2456-2602.

27. Narasimhappa, M., Mahindrakar, A. D., Guizilini, V. C., Terra, M. H., & Sabat, S. L., *MEMS-Based IMU Drift Minimization: Sage Husa Adaptive Robust Kalman Filtering*. IEEE SENSORS JOURNAL, 2020. 20(1): p. 250-260.

28. Li, D., Zhang, Z. S., Liu, P., Wang, Z. P., & Zhang, L., *Battery Fault Diagnosis for Electric Vehicles Based on Voltage Abnormality by Combining the Long Short-Term Memory Neural Network and the Equivalent Circuit Model*. IEEE TRANSACTIONS ON POWER ELECTRONICS, 2021. 36(2): p. 1303-1315.

29. Liu, R. X., & Zhang, C. L., *An Active Balancing Method Based on SOC and Capacitance for Lithium-Ion Batteries in Electric Vehicles*. FRONTIERS IN ENERGY RESEARCH, 2021. 9: p. 569-652.

30. Liu, Q. H., & Yu, Q. Q., *The lithium battery SOC estimation on square root unscented Kalman filter*. ENERGY REPORTS, 2022. 8: p. 286-294.

31. Qian, K. F., & Liu, X. T., *Hybrid optimization strategy for lithium-ion battery's State of Charge/Health using joint of dual Kalman filter and Modified Sine-cosine Algorithm*. JOURNAL OF ENERGY STORAGE, 2021. 44: p. 2564-2896.

32. Qays, M. O., Buswig, Y., Hossain, M. L., & Abu-Siada, A., *Recent Progress and Future Trends on the State of Charge Estimation Methods to Improve Battery-storage Efficiency: A Review*. CSEE JOURNAL OF POWER AND ENERGY SYSTEMS, 2022. 8(1): p. 105-114.

33. Li, L. L., Liu, Z. F., & Wang, C. H., *The Open-Circuit Voltage Characteristic and State of Charge Estimation for Lithium-Ion Batteries Based on an Improved Estimation Algorithm*. JOURNAL OF TESTING AND EVALUATION, 2020. 48(2): p. 1712-1730.

34. Liu, Y. Y., Cai, T. T., Liu, J. B., Gao, M. Y., & He, Z. W., *State of Charge Estimation for Li-Ion Batteries Based on an Unscented H-Infinity Filter*. JOURNAL OF ELECTRICAL ENGINEERING & TECHNOLOGY, 2020. 15(6): p. 2529-2538.

35. Movassagh, K., Raihan, A., Balasingam, B., & Pattipati, K., *A Critical Look at Coulomb Counting Approach for State of Charge Estimation in Batteries*. ENERGIES, 2021. 14(14): p. 235-426.

36. Liu, Y. F., Li, J. Q., Zhang, G., Hua, B., & Xiong, N., *State of Charge Estimation of Lithium-Ion Batteries Based on Temporal Convolutional Network and Transfer Learning*. IEEE ACCESS, 2021. 9: p. 34177-34187.

37. Zhuang, S. Q., Gao, Y., Chen, A. D., Ma, T. Y., Cai, Y., Liu, M., & Ke, Y. M., *Research on Estimation of State of Charge of Li-ion Battery based on Cubature Kalman Filter*. JOURNAL OF THE ELECTROCHEMICAL SOCIETY, 2022. 169(10): p. 564-584.

38. Yu, P., Wang, S. L., Yu, C. M., Jiang, C., & Shi, W. H., *An adaptive fractional-order extended Kalman filtering for state of charge estimation of high-capacity lithium-ion battery*. INTERNATIONAL JOURNAL OF ENERGY RESEARCH, 2022. 46(4): p. 4869-4878.

39. Huang, C., Yu, X. Y., Wang, Y. C., Zhou, Y. Q., & Li, R., *State of charge estimation of li-ion batteries based on the noise-adaptive interacting multiple model*. ENERGY REPORTS, 2021. 7: p. 8152-8161.

40. Qian, Y. M., Zheng, J., Ding, K., Zhang, H., Chen, Q., Wang, B., Wang, Y., & Huang, Z. R., *Fast Open Circuit Voltage Estimation of Lithium-Ion Batteries Using a Relaxation Model and Genetic Algorithm*. IEEE ACCESS, 2022. 10: p. 96643-96651.

41. Zhou, L., Lai, X., Li, B., Yao, Y., Yuan, M., Weng, J. H., & Zheng, Y. J., *State Estimation Models of Lithium-Ion Batteries for Battery Management System: Status, Challenges, and Future Trends*. Batteries-Basel, 2023. 9(2): p. 458-478.

42. Qi, C. S., Wang, S. L., Cao, W., Shi, H. T., & Xie, Y. X., *A Novel Multi-Constraint Peak Power Prediction Method Combined with Online Model Parameter Identification and State-of-Charge Co-Estimation of Lithium-Ion Batteries*. JOURNAL OF THE ELECTROCHEMICAL SOCIETY, 2022. 169(12): p. 220-239.

43. Zhang, W. J., Wang, L. Y., Wang, L. F., Liao, C. L., & Zhang, Y. W., *Joint State-of-Charge and State-of-Available-Power Estimation Based on the Online Parameter Identification of Lithium-Ion Battery Model*. IEEE TRANSACTIONS ON INDUSTRIAL ELECTRONICS, 2022. 69(4): p. 3677-3688.